First and Second Reductions in an Aprotic Solvent: Comparing Computational and Experimental One-electron Reduction Potentials for 345 Quinones

Sarah El Hajj and Samer Gozem*

Department of Chemistry, Georgia State University, Atlanta, Georgia, 30302, United States

E-mail: sgozem@gsu.edu

Abstract

Using reference reduction potentials of quinones recently measured relative to the saturated calomel electrode (SCE) in N,N-dimethylformamide (DMF), we benchmark absolute one-electron reduction potentials computed for 345 $Q/Q^{\bullet-}$ and 265 $Q^{\bullet-}/Q^{2-}$ reactions using adiabatic electron affinities computed with density functional theory and solvation energies computed with three continuum solvation models; IEF-PCM, COSMO, and SM12. Regression analyses indicate a strong linear correlation between experimental and absolute computed $Q/Q^{\bullet-}$ reduction potentials with Pearson's correlation coefficient r between 0.95-0.96 and mean absolute error (MAE) relative to the linear fit between 83.29-89.51 mV for different solvation methods when the slope of the regression is constrained to one. The same analysis for $Q^{\bullet-}/Q^{2-}$ gave a linear regression with r between 0.74-0.90 and MAE between 95.87-144.53 mV, respectively. The y-intercept values obtained from the linear regressions are in good agreement with the range of absolute reduction potentials reported in the literature for the SCE

but reveal several sources of systematic error. The y-intercepts from $Q^{\bullet-}/Q^{2-}$ calculations are lower than those of $Q/Q^{\bullet-}$ by around 400 mV for PCM and SM12 and 200 mV for COSMO. Systematic errors also arise between molecules having different ring sizes (benzoquinones, naphthoquinones, and anthraquinones) and different substituents (titratable vs. non-titratable). SCF convergence issues were found to be a source of random error that were slightly reduced by directly optimizing the solute structure in the continuum solvent reaction field. While SM12 MAEs were lower than those of PCM and COSMO for $Q/Q^{\bullet-}$, SM12 had larger errors for $Q^{\bullet-}/Q^{2-}$ pointing to a limitation when describing multiply charged anions in DMF. Together, the results highlight the advantage of—and further need for—testing computational methods using a large experimental data set that is not skewed (e.g., having more titratable than non-titrable substituents on different parent groups or vice versa) to help further distinguish between sources of random and systematic errors in the calculations.

Introduction

Electron transfer reactions are ubiquitous processes in redox reactions[1,2] such as photocatalysis,[3] photobiocatalysis,[4–6] electrocatalysis,[7–9] sensing,[10–12] energy harvesting,[13,14] and flow batteries.[15,16] The fundamental thermodynamic quantity that determines the driving force for redox reactions to occur is the redox potential.[17] The redox potential, typically measured by cyclic voltammetry when a molecule exhibits a reversible voltammetric wave,[18] determines the propensity of that molecule to accept or donate electrons.[17,19,20]

Computations provide a distinct route to predicting redox potentials from first principles. Such calculations, when predictive, can be used to simulate redox properties of new materials or to determine potentials for systems in difficult experimental conditions such as for non-reversible redox reactions or highly unstable species.[20,21]

Quinones are a class of conjugated redox-active molecules derived from aromatic compounds and containing two carbonyls in a cyclic arrangement.[22] In aprotic solvent, neutral

quinones can undergo a one-electron reduction to a radical anionic semiquinone ($Q^{\bullet-}$). The semiquinone can undergo further one-electron reduction to an aromatic dianion (Q^{2-}).[23–26] In aqueous or protic media, the same reduction is often coupled to a proton transfer resulting in neutral semiquinone ($QH^{\bullet}$) or hydroquinone (QH_2) species.[17,19,24]

Due to their redox characteristics, quinones and their derivatives play a critical role in biological processes such as respiration and photosynthesis.[23,27,28] They serve as important scaffolds for synthesis of clinically approved drugs for treating cancer (e.g., Adriamacyin and Cerubidine),[29–32] diabetes,[33] and cardiovascular diseases,[34] among others.[35] Quinones have also been used in applications ranging from energy storage,[36,37] natural dyes (e.g., 2-hydroxy-1,4-naphthoquinone, or Henna),[29,38–40] and synthetic dyes (e.g., Disperse Red 9, or 1-(methylamino)-anthraquinone, used in bank security dye packs that get activated upon bank robberies).[41]

Most computations apply a thermodynamic cycle to compute redox potentials.[17] There are several important ingredients for such calculations to be accurate. Chief among them, the solvation model used must have a balanced description of the solvation of the oxidized and reduced species. Therefore most benchmark studies have placed a heavy emphasis on testing solvation models for redox potential calculations.

Multiple redox benchmark studies have indicated that calculations are accurate to within a fraction of a volt relative to experiments. Coote and co-workers[19] studied thirteen $Q/Q^{\bullet-}$ reduction potentials of para-quinones in a non-aqeuous solvent, acetonitrile. They employed the composite G3(MP2)-RAD approach for the gas phase calculations and Hartree Fock (HF) or B3LYP solvation energy calculations with the conductor-like polarizable continuum model (C-PCM). They found that the HF and B3LYP solvation gave a mean absolute deviation (MAD) of 70 mV and 120 mV compared to experimental redox potentials, respectively. They also tested the effect of using B3LYP for the gas-phase calculations, applying a constant correction factor of 280 mV derived by Guo and co-workers[20] on the basis of ionization energy calculations, which they suggest would also be applicable to electron affinities. Guo

and co-workers[20] studied both gas phase ionization potentials (IPs) and oxidation potentials of 270 diverse organic molecules and showed that using a density functional theory (DFT) with polarable continuum model (PCM) gave an average error of 170 mV in acetonitrile after a constant shift of 280 mV applied to the IPs. Leszczynski and co-workers[42] tested several different density functionals and solvation methods for calculating $Q/Q^{\bullet-}$ reduction potentials of several classes of molecules, including nine quinones, with MADs ranging from 30 to 300 mV. Grimme and co-workers compiled a set of 313 reduction and oxidation potentials (313ROP) for organic and organometallic compounds in various solvents, and use the data to benchmark semi-empirical quantum mechanical methods with implicit solvation.[43]

Several studies have also employed explicit solvation for computing reduction potentials of quinones. Zimmerman and co-workers[44] found that DFT with implicit solvation generally worked well for $Q/Q^{\bullet-}$ reduction potentials, but in a few high error outliers using explicit (QM/MM) solvation reduced the errors significantly from 194 mV to 8 mV. They also found that implicit solvation gave a much larger MAD for $Q^{\bullet-}/Q^{2-}$ reduction potentials in acidic aqeuous conditions. These errors were reduced by including in the simulation a counterion that stabilizes the anionic species. Ghosh *et al.*[45] and Tazhigulov *et al.*[46] presented protocols for accurate prediction of redox potentials using *ab initio* wave function methods with an effective fragment potential (EFP) to describe the solvent.[47]

More recently, several groups have applied machine learning (ML) approaches to model redox potentials. Liu and co-workers[48] used ML to reduce errors from DFT redox potential calculations and tested it on Grimme's ROP313 data set of organic and organometallic compounds. They found out that with the best performing ML corrections, errors were reduced by 23-49%, reducing the MAE from 430 mV to 220 mV. They also found out that ML is less sensitive to the DFT functional used.

The current study benchmarks theoretical calculations for 345 $Q/Q^{\bullet-}$ and 265 $Q^{\bullet-}/Q^{2-}$ reduction potentials of quinones in an aprotic solvent. While it is desirable to test computational protocols against experimental data for a wide range of different molecules, as done for

instance in the ROP313 set, here we take a different approach; we study a large data set of reduction potentials consisting of closely related organic molecules that have been measured using a common experimental setup and conditions. All the experimental reference data used in this work were recently reported in a study by Prince, Dutton, and Gunner.[29] The quinones range in size from 12 to 153 atoms, and include several substituents including alkyl chains, halogens, polar protic and aprotic groups, and even charged groups like sulfonates. Having a large data set from a single source reduces the likelihood of random errors associated with different equipment and human error. The aprotic solvent conditions in which the experiments were carried out simplify calculations on the one hand, since they mitigate proton transfer with the solvent, but also pose a challenge to continuum solvation models that typically do not perform as well for low dielectric constants as for aqueous solvation.[19,49] Furthermore, the focus on both sequential $Q/Q^{\bullet-}$ and $Q^{\bullet-}/Q^{2-}$ potentials allows for a more stringent test of electronic structure methods and solvation models that must treat neutral, radical anionic, and dianionic solutes in a balanced way.

The aim of this study is to recognize sources of random and systematic errors in widely used density functional theory and implicit solvation model methods in redox potentials of sequential one-electron reductions. Understanding the sources of these errors can help correct for them or develop improved computational methods and protocols.

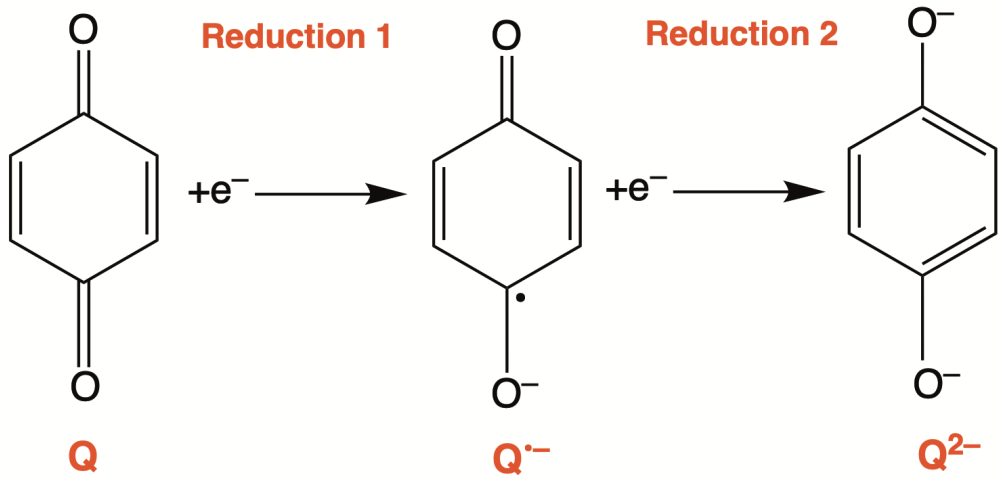

Scheme 1: Quinone reduction in aprotic solvent.

Computational Methods

Experimental $Q/Q^{\bullet-}$ and $Q^{\bullet-}/Q^{2-}$ reduction potentials were reported recently by Prince *et al.* in dry N,N-dimethylformamide (DMF) solvent against a saturated calomel electrode (SCE) reference.[29] Most molecules are derivatives of three parent quinones: 1,4-benzoquinone (BQ), 1,4-naphthoquinone (NQ), and 9,10-anthraquinone (AQ). A few other quinone isomers or related aromatic non-quinones are also included ("Others"). Specifically, Prince *et al.* reported experimental reduction potentials for 117 substituted BQs, 90 substituted NQs, 110 substituted AQs, and 33 miscellaneous quinones and non-quinones; in total, 350 molecules.[29] In Table S1, we list those 350 molecules using indices 000 to 349 and include their chemical structures. Of those 350, we exclude 5 molecules from the analysis in this work: 3,x-dichloro-2-methoxycarbonyl-1,4-benzoquinone (116), for which no structure could be found, Doxorubicin (209) and Cerubidine (210), which we identified as duplicates of Adriamycin (192) and Cerubidine (193), and 2-methoxy-3-amino-5-methyl-6-decaprenyl-1,4-benzoquinone (094) and Reactive blue (164). The last two were excluded due to their high molecular weight, rendering the computations intractable. This resulted in a total of 345 $Q/Q^{\bullet-}$ reduction potentials. Experimental $Q^{\bullet-}/Q^{2-}$ reduction potentials were not reported for 80 out of the 345 molecules,[29] so we have 265 $Q^{\bullet-}/Q^{2-}$ reduction potentials.

Quantum chemical calculations employed Density functional theory (DFT) with the Becke-3 Lee-Yang-Parr (B3LYP)[50,51] functional and the 6-311++G(d,p)[52] split-valence triple-ζ basis set. Unrestricted B3LYP was used for the open-shell one-electron reduced radicals. This combination of method and basis set is a popular choice that has been tested extensively for quinones in combination with implicit solvation.[24,53,54] A mixed basis set was used for iodine-containing molecules, treating iodine with the def2TZVP basis set with an effective core potential[55] and remaining atoms with 6-311++G(d,p). Frequency calculations were used to check for imaginary frequencies. If imaginary frequencies were found, the structure was displaced along the scaled normal mode vector corresponding to that frequency and re-optimized until all positive frequencies were obtained.

Throughout this work, we refer to the the initial (oxidized) quinone as the neutral quinone Q, the one-electron reduced species as the radical anion $Q^{\bullet-}$, and the fully reduced quinone as a dianion Q^{2-}. However, several molecules included in this work have charged substituents such as sulfonates. In those cases, an additional negative charge is included in the computations, but we continue to use the $Q/Q^{\bullet-}/Q^{2-}$ nomenclature for convenience, as these refer to the charge and oxidation state of the quinone backbone.

Since DMF is an aprotic solvent, we assume that all alkaline substituents such as amines (which are mostly anilines and therefore weak bases), remain deprotonated. Weak acids, such as alcohols, were kept protonated. However, sulfonates ($R-SO_3^-$) are kept deprotonated because they are strong acids.

Solvation energies in DMF were computed using three implicit solvation methods: a polarizable continuum model (PCM)[56–58] using the integral equation formalism (IEF-PCM),[57] a COnductor-like Screening MOdel (COSMO),[59] and SM12.[60–62] In the case of PCM, we tested the effect of using a single-point energy calculation on the gas-phase optimized geometries (PCM-cycle) as well as re-optimizing the molecule with PCM solvation (PCM-direct). On the other hand, COSMO and SM12 calculations were only carried out as single-point energy calculations on the gas-phase optimized geometries (i.e., using the thermodynamic cycle).

Gas-phase and IEF-PCM calculations, including geometry optimizations, were computed with the Gaussian16 software package.[63] COSMO and SM12 solvation energies were computed with the Q-chem 5.4 software package.[64] SM12 calculations were parameterized based on CM5 partial atomic charges.[60,65] For the COSMO calculations, a dielectric constant of 37.219 was used for DMF, obtained from the Minnesota Solvent Descriptor Database.[66]

In both Gaussian and Q-Chem, SCF convergence issues were encountered frequently for the doubly reduced states, especially in the gas phase were such states may be metastable. Those issues were resolved using SCF convergence options available in both software packages. Specifically, in Gaussian, we employed the YQC convergence option that performs

linear searches and then switches to a default or quadratically convergent algorithm to complete the convergence.[67] When that fails, SCF convergence is achieved with another method first and used as a guess for B3LYP. In Q-Chem, we used different SCF starting guess orbitals and/or changed the SCF algorithm until convergence. For SM12 calculations, the solvent self-consistent field procedure did not converge correctly for three anions, so the Merz-Singh-Kollman[68,69] (for molecules 085 and 299) or CHELPG[70] (for molecule 050) atomic charge models were used instead of CM5.

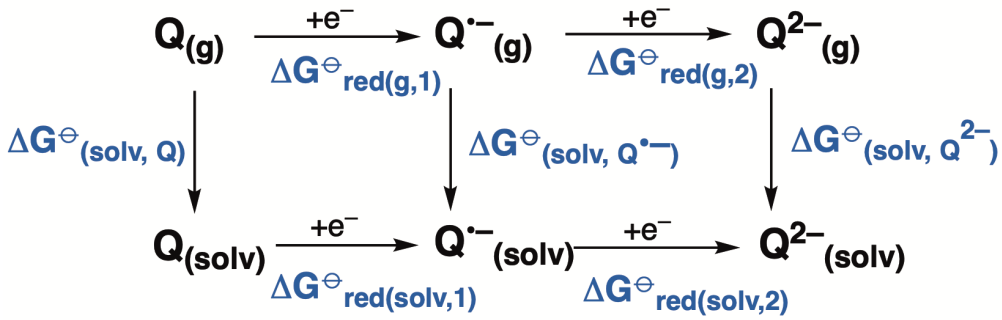

Scheme 2: Born-Haber Thermodynamic cycle[17] for one-electron reduction: From neutral to anionic semiquinone (Reduction 1) and from anionic semiquinone to the two-electron reduced dianionic quinone (Reduction 2). The upper leg shows gas-phase reduction free energies; the lower leg shows reduction free energies in solvent. Those two legs are connected by solvation free energy calculations (arrows pointing down).

From the thermodynamic cycle in Scheme 2, the free energy of reduction in solvent can be computed using:

$$\Delta G^{\ominus}_{\mathrm{red(solv,1)}} = \Delta G^{\ominus}_{\mathrm{red(g,1)}} + \Delta G^{\ominus}_{\mathrm{(solv,Q^{\bullet -})}} - \Delta G^{\ominus}_{\mathrm{(solv,Q)}} \tag{1}$$

$$\Delta G^{\ominus}_{\mathrm{red(solv,2)}} = \Delta G^{\ominus}_{\mathrm{red(g,2)}} + \Delta G^{\ominus}_{\mathrm{(solv,Q^{2-})}} - \Delta G^{\ominus}_{\mathrm{(solv,Q^{\bullet -})}} \tag{2}$$

$\triangle G^{\ominus}_{\mathrm{red(solv,1)}}$ and $\triangle G^{\ominus}_{\mathrm{red(solv,2)}}$ represent the free energy due to reduction in solution of Q to $Q^{\bullet-}$ and $Q^{\bullet-}$ to Q^{2-}, respectively. $\triangle G_{\mathrm{red(g,1)}}$ is calculated by taking the difference of the sums of the electronic energies and thermal correction to Gibbs free energy of the reduced and oxidized forms.[19,44,71,72] The thermal corrections are obtained from the frequency calculations of the gas-phase optimized structures. The reduction free energies are related to the absolute

reduction potentials:

$$E^{\ominus,\mathrm{abs}}_{\mathrm{calc},1} = -\frac{\triangle G^{\ominus}_{\mathrm{red(solv,1)}}}{nF} \quad (3)$$

$$E^{\ominus,\mathrm{abs}}_{\mathrm{calc},2} = -\frac{\triangle G^{\ominus}_{\mathrm{red(solv,2)}}}{nF} \quad (4)$$

where n represents the number electrons (here, 1) gained by the quinone from the electrode, and F is Faraday's constant, 23.061 kcal mol^{-1} V^{-1}.[73] $E^{\ominus\mathrm{abs}}_{\mathrm{calc},1}$ and $E^{\ominus\mathrm{abs}}_{\mathrm{calc},2}$ represent the absolute theoretically predicted values of the standard potentials for reductions 1 and 2 respectively. We report all reduction potentials in units of mV.

The reduction potentials in Eq. 3 and 4 are absolute potentials and therefore represent the Gibbs free energies required to bring a free electron from vacuum and add it to the molecule. On the other hand, the experimental reduction potentials were measured by Prince *et al.* under standard conditions relative to the SCE reference.[29] To compare the computed reduction potentials to the experimental ones, it is necessary to subtract the absolute reduction potential of the SCE under the same conditions. Specifically, for reduction 1 and reduction 2:[74]

$$E^{\ominus,\mathrm{SCE,DMF}}_{\mathrm{calc},1}(\mathrm{mV}) = E^{\ominus,\mathrm{abs}}_{\mathrm{calc},1}(\mathrm{mV}) - E^{\mathrm{abs,DMF}}_{\mathrm{SCE,ref}}(\mathrm{mV}) \quad (5)$$

$$E^{\ominus,\mathrm{SCE,DMF}}_{\mathrm{calc},2}(\mathrm{mV}) = E^{\ominus,\mathrm{abs}}_{\mathrm{calc},2}(\mathrm{mV}) - E^{\mathrm{abs,DMF}}_{\mathrm{SCE,ref}}(\mathrm{mV}) \quad (6)$$

$E^{\mathrm{abs,\ DMF}}_{\mathrm{SCE,ref}}$ represents the absolute reduction potential of the SCE which is the free energy change associated with the the reference SCE anodic half-reaction ($\frac{1}{2}\,\mathrm{Hg_2Cl_2(s)} + \mathrm{e^-} \longrightarrow \mathrm{Hg(l)} + \mathrm{Cl^-}$). The SCE potential is typically reported relative to the standard hydrogen electrode (SHE), $\frac{1}{2}\,\mathrm{H^+(aq)} + \mathrm{e^-} \longrightarrow \frac{1}{2}\,\mathrm{H_2}$. However, determining the absolute reduction potential of the SHE, and therefore SCE, is not trivial and has remained a topic of debate in the literature.[74–80]

Much of this debate revolves around the theoretical treatment of the proton hydration energy and free electron energy terms through work functions that account for surface effects. IUPAC recommended an SHE absolute potentials close to 4.44 V.[81] However, Kelly *et al.*[71,82] and Isse *et al.*[74] argue that a more suitable computational reference should use the standard hydration free energy of the proton instead of the real potential at the gas/liquid interface, since the latter includes an energy contribution related to the surface potential at the interface between the two phases. They arrive at a reduction value of 4.28 V for the SHE. Recent computational studies have continued to indicate good agreements between computed and experimental redox potentials using a SHE reference of 4.44 V.[79,83] Recently, Williams *et al.* obtained via nano-calorimetry techniques new values for the absolute standard hydrogen electrode ranging from 4.11 V[84] to 4.2 V[85,86] while Shigeta *et al.* computed SHE's potential to be 4.48 V[83] and 4.52 V.[87]

In addition to the difficulty in knowing the absolute potential of the SHE reference, determining the relative potential of SCE to SHE for a non-aqueous solution is complicated by liquid junction potentials arising from differing ion mobilities in different solutions. Experimentally, such reduction potentials are sensitive to the solvent, electrolytes, and environmental factors, which may result in difficulties with reproducibility.[72,88,89] Isse *et al.*, using a reduction potential of 4.281 V for SHE, +0.241 V potential for aqueous SCE vs. SHE, and 0.172 V liquid junction potential reported by Diggle and Parker for DMF solvent,[90] arrive at an absolute reduction potential of 4.350 V for SCE with DMF.[74]

Often, this issue of absolute potentials can be avoided by using an internal reference such as the ferrocene/ferricenium redox couple.[72] This led to multiple attempts to model the absolute reduction potential of ferrocene accurately.[91,92] Prince *et al.*[29] reported the reduction potential for ferrocene vs. SCE as +524 mV using their experimental setup and conditions. Similarly, several studies reported computed hydrogen electrode (CHE) values as a reference.[93,94] Since ferrocene and H_2 have very different electronic and molecular structure than quinones, we did not use them in this study as an internal computational reference.

In light of the uncertainties surrounding the absolute reduction potential of SCE, we followed a similar approach as some others have done[79,95] and opted to report a direct correlation between the absolute theoretically calculated reduction potentials compared to the experimental values vs SCE. The computational values will therefore be offset from the experimental data by a constant reflected in the y-intercept. This constant, a fitted parameter, corresponds to the absolute reduction potential of the SCE if we assume no systematic errors in the calculations. However, systematic errors that arise in our calculations will be also absorbed by this fitted y-intercept on top of the SCE offset. Since we cannot determine with certainty the magnitude of this systematic error, we cannot determine the exact SCE value. However, due to the large dataset of 610 reduction potentials (345 $Q/Q^{\bullet-}$ and 265 $Q^{\bullet-}/Q^{2-}$), we can compare subsets of this data to disentangle some sources of random errors (reflected by the MAE) and systematic errors (reflected by the y-intercepts).

Data Availability

The calculation of 345 $Q/Q^{\bullet-}$ and 265 $Q^{\bullet-}/Q^{2-}$ reduction potentials using different solvation methods requires thousands of quantum chemical calculations and their analysis. Therefore, the workflow and data analysis were largely automated through a series of Python and Bash scripts made available in a GitHub repository, https://github.com/gozem-gsu/Redox-Potential-Protocol The repository also includes the B3LYP/6-311++G(d,p) optimized geometries of the 345 molecules in different redox states and all the data generated in this work. These scripts can be readily adopted to test different methods, basis sets, solvation models, or different molecules and properties.

Briefly, the workflow follows these steps:

Algorithm 1 Automated steps for computing redox potentials

1: Obtain SMILES string from molecule CAS number (if available) using CIRpy.
2: Convert the SMILES string into 3D molecular structures in Cartesian coordinates using RDKit.[96]
3: For molecules without CAS numbers, generate initial coordinates using IQmol.
4: Initialize submitting gas-phase optimization jobs simultaneously by preparing necessary input files for each of the neutral, radical, and anionic state of every molecule.
5: Check for output file errors. In case of SCE convergence errors, resubmit with different SCF convergence algorithm.
6: Check for negative frequency occurrences. In case of negative frequencies, resubmit optimization from last geometry displaced along a scaled normal modes.
7: Extract gas-phase optimized coordinates.
8: Run single-point solvation energy calculations.
9: Extract the gas-phase and solvent electronic energies and thermal correction to Gibbs free energy and use them to calculate reduction potentials for $Q/Q^{\bullet-}$ and $Q^{\bullet-}/Q^{2-}$.

Statistical Analysis

Experimental and computed redox potentials for the four solvation models (PCM-cycle, PCM-direct, COSMO, SM12) and for each of the two reduction reactions ($Q/Q^{\bullet-}$ and $Q^{\bullet-}/Q^{2-}$) were plotted and fit using a linear regression with the slope constrained to 1. As discussed in the Methods section, computed redox potentials are absolute potentials, while the experimental redox potentials were measured relative to SCE.

The computed and experimental data have different standard deviations; $\sigma_{exp} = 334$ mV while σ_{comp} varies from 390 to 401 mV for different solvation models in the case of $Q/Q^{\bullet-}$, and $\sigma_{exp} = 254$ mV while σ_{comp} varies from 284 to 299 mV for different solvation models for $Q^{\bullet-}/Q^{2-}$. The wider distribution of computed potentials can be attributed to systematic errors and outliers in the computed data.

The BQ, NQ, AQ, and Other redox potentials were all fit together using a general linear regression for all molecules. Then, the four parent groups (BQ, NQ, AQ, and Other) were fit separately.

If the $Q/Q^{\bullet-}$ and $Q^{\bullet-}/Q^{2-}$ calculations and experiments for the four groups (BQ, NQ, AQ, and Other) are of similar quality, it is expected that they should give similar y-intercepts

and MAEs. Therefore, fitting the data both ways (together and individually) helps delineate possible sources of random and systematic error in the different groups.

Among the arsenal of statistical tools available, we chose to quantify the discrepancy between computed and experimental values using two metrics: the Pearson correlation coefficient,

$$r = \frac{\sum (x_i - \bar{x})(y_i - \bar{y})}{\sqrt{\sum (x_i - \bar{x})^2 \sum (y_i - \bar{y})^2}}, \tag{7}$$

and the Mean Absolute Error (MAE, in mV),

$$\mathrm{MAE} = \frac{1}{N} \sum_{i=1}^{N} |E_{\mathrm{fit}} - E_{\mathrm{exp}}|. \tag{8}$$

The first metric, r, represents the linearity of the correlation between computed and experimental potentials. The second metric, the MAE, represents the average deviation of the data from the idealized (linear) fit. This is not a deviation from the experimental data, which is not used here since those are offset by the SCE absolute potential. Those two metrics were chosen, along with the choice to constrain the slope to 1, because they are invariable to the choice of reference axis (experimental vs. computed). Other widely used metrics, such as the coefficient of determination (R^2), depend on a null hypothesis that is sensitive to the standard deviation of the data.

All metrics were calculated using Scikit-learn library version 1.2.2 using sklearn.metrics[97] module or numpy version 1.25.2.

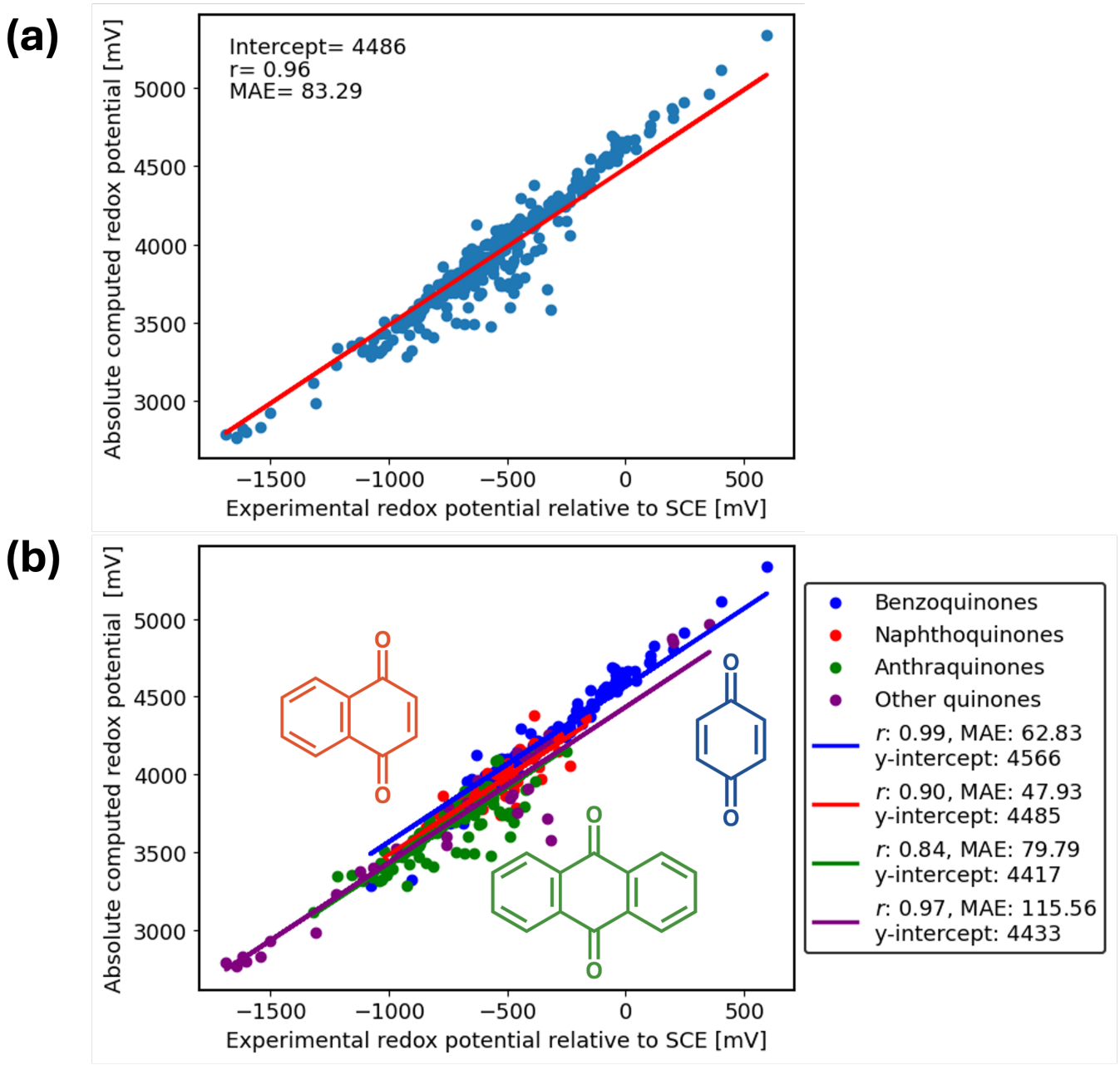

Figure 1: (a) Correlation between $Q/Q^{\bullet -}$ experimental reduction potentials relative to SCE and absolute calculated reduction potentials for N = 345 total studied quinone derivatives in DMF using the **PCM-cycle** approach. (b) Correlation between experimental reduction potentials and absolute calculated ones fitted separately for 4 groups: 115 Benzoquinones (blue), 90 Naphthoquinones (red), 107 Anthraquinones (green), and 33 Others (purple). Experimental data were obtained from Prince *et al.*[29]

Results and discussion

$Q/Q^{\bullet-}$ Reduction Potentials

The correlation between experimental $Q/Q^{\bullet-}$ reduction potentials relative to the SCE and the absolute computed reduction potentials is illustrated in Fig. 1. In this figure, we constrained the slope to 1.00. The linear fit gives an r value of 0.96, MAE of 83.29 mV, and a y-intercept of 4486 mV, as shown in Fig. 1(a). If we assume that the SCE reduction potential is 0.2412 V above SHE in aqueous media[89,98] and a liquid junction potential of 0.172 V for DMF with tetraalkylammonium salts,[90] this means that SCE in DMF has a reduction potential of 0.069 V relative to SHE. A value of 4.486 V for SCE translates to 4.417 V for SHE. The standard deviation associated with this value is 0.092 V (based on the standard deviation of data relative to the fit). 4.417 V lies between the commonly used values of 4.28 V and 4.44 V.[71,74,81,82] However, any systematic errors in the gas phase electron affinity calculations and in the solvation energies are reflected in this value.

A linear regression analysis without any constraint instead yields a slope of 1.1491 and a lower MAE of 69.76, as shown in Fig. S1(a). The large slope is unphysical and indicative of a systematic error in the calculations, reflecting a larger variance in the computed reduction potentials compared to the experimental ones.

To better understand the source of this error, we plot in Fig. 1(b) the linear regression analysis for BQ, NQ, AQ, and other quinones separately. We notice two trends; firstly, the different groups have different average redox potentials, with BQ on average having higher (more positive) reduction potentials than NQ and with AQ having the lowest potentials. Secondly, the y-intercepts follow the same trend if the slope is constrained to 1: BQ > NQ > AQ. This is indicative of a systematic error that is different for each group. Comparing Fig. S1(a) and Fig. 1(b), we can now attribute the larger-than-one slope in plot S1(a) to a systematic error related to the length of the conjugation or the ring size of the quinone. This error is not related to the total size of the system (i.e., including substituents); when

accounting for substituents, the average size of BQs, NQs, AQs, and other quinones are comparable, with an average size of 29 atoms, 30 atoms, 35 atoms, and 27 atoms, respectively. Moreover, a plot of individual absolute errors (relative to the fit) vs. atom size yields a plot with no linear correlation ($R^2 = 0.002$ for a linear regression).

In Fig. S1(b), we include a linear regression analysis for BQ, NQ, AQ, and other quinones separately but without constraining the slope to 1. We find that the slope now varies considerably for the different subgroups (1.195 for BQ, 0.964 for NQ, 0.859 for AQ, and 1.041 for Others). Since the slope is not always larger than 1 within each group, this again indicates that the overall slope, 1.1491 in Fig. S1(a), is related to the ring size and is not a constant overestimation for all systems. This error may originate from the gas-phase electron affinity calculations; DFT has been shown to exhibit size-dependent errors for ionization potentials.[99]

Next, we report on the random error. From Fig. 1(b), NQs exhibit a lower MAE (47.93 mV) compared to BQs (62.83 mV), which, in turn, is lower than AQs (79.79 mV). However, when the slope is not constrained to 1 (S1(b)), the trend in MAEs increases with the ring size (43.34 mV for BQ, 48.54 mV for NQ, 77.35 mV for AQ, and 113.56 mV for others). This change in trend is tied to the different slopes of the subgroups; for example, NQ has a slope closest to unity in Fig. S1(b), and therefore the MAE remains small when the slope is constrained to 1.

There are several factors that could contribute to the different intrinsic slopes and MAEs of the different groups. One of those factors is the nature of the substituents. For example, protic substituents may be involved in hydrogen-bonding interactions or even acid/base chemistry which are not properly captured by implicit solvation models.[44] While the measurements by Prince *et al.* were carried out in aprotic solvent and care was taken to minimize the amount of moisture,[29] even a few millimolars of water can alter the apparent reduction potential of quinones in DMF.[100] Therefore, such systems may give larger errors that are more pronounced for protic quinones. This is supported by the data in Table 1, where titrat-

able quinones give, on average, larger MAEs than non-titratable quinones. In the table, we categorized quinones as titratable if they have a group that may act as an acid or base, such as amines, alcohols, sulfonates, and as non-titratable if they only have groups such as halogens, nitro, cyano, and acetoxy. The "Other" quinones are the only group that does not follow the MAE(titratable) > MAE(non-titratable) trend because it constitutes a small sample size with several bulky outliers that skew the errors. Another trend emerges in Table 1: The number of titratable and non-titratable residues are not equally divided among the parent quinones, which introduces a bias; BQ has mostly non-titratable substituents, NQ has an equal number of titratable and non-titratable substituents, and AQs have mostly titratable residues. Ideally, the three groups should be tested having similar substituent types. However, likely due to factors such as ease of synthesis, stability, and solubility, the nature of the substituents on BQ, NQ, and AQ are not the same. This serves as a possible explanation for why the MAEs increase across the series BQ < NQ < AQ (when slope is not constrained to 1).

Table 1: MAEs for $Q/Q^{\bullet-}$ reduction potentials for molecules with titratable versus non-titratable subsituents using the PCM-cycle approach. N represents the total number of titratable or non-titratable molecules across all quinones, or across every parent subgroup.

	MAEs for all	**MAEs for BQs**	**MAEs for NQs**	**MAEs for AQs**	**MAEs for others**
Titratable	83.9 (N=140)	107.2 (N=16)	57.6 (N=45)	93.7 (N=68)	96.6 (N=11)
Non-titratable	55.7 (N=205)	55.9 (N=99)	41.3 (N=45)	55.6 (N=39)	125.0 (N=22)

In SI Table 2, we further break down the errors associated with different substituents. We find in particular that, cyano, sulfonates, acetoxy, amine and hydroxy groups have a higher MAE than the computational average for all quinones, whereas halogens, nitro, oxy, and thio substituents give MAEs below the average. Such errors may not always be systematic; several anecdotal examples suggest that errors are not easy to predict from structure. The molecules that give the largest errors, such as 333 and 334 (absolute error relative to fit of 591 mV and 441 mV, respectively) have pyramidalized aromatic rings due to bulky isoproyl

and tetrabutyl substituents adjacent to each other, which induce a large steric strain on the quinone ring. Anthraquinones with several hydroxy groups such as 203 and 207 (absolute error relative to fit of 443 mV and 316 mV, respectively) also tend to give large errors due to intramolecular hydrogen bonding and proton rearrangements upon reduction. Another molecule, 1-amino-2-sulfonate-9,10-anthraquinone (ID 157), has a large error relative to fit of 399 mV. Introducing a bromo group para to the amine (1-amino-4-bromo-2-sulfonate-9,10-anthraquinone, ID 163) reduces the error considerably to 4 mV. While one potential explanation is that the bromo group reduces the basicity of the amino group through its electron-withdrawing character, this example, along with the previous two, demonstrate the difficulty in trying to correlate source of error for reduction potentials to structural elements such as substituents.

Next, we test the effect of carrying out the optimization and frequency calculations directly in the continuum solvent reaction field. This approach, referred to as PCM-direct instead of PCM-cycle, does not appreciably change the results of the calculation for $Q/Q^{\bullet-}$ reductions (Fig. S2). We also test two other solvation models, COSMO and SM12. The linear regressions, analogous to Fig. 1, are shown in Figures S3 and S4 in the SI. In Fig. 2, we summarize the results of the linear regressions by comparing the MAEs and y-intercept values fitted by the different models. Generally, the MAEs for the different solvent models are comparable. However, COSMO solvation results in y-intercept values that are 180-280 mV higher than the other solvation models. This is consistent with a recent benchmark study by Tomanik *et al.*[79] which indicates an optimal fitted value for the SHE absolute potential that is between 160 mV and 320 mV higher for COSMO compared to PCM for different data sets.

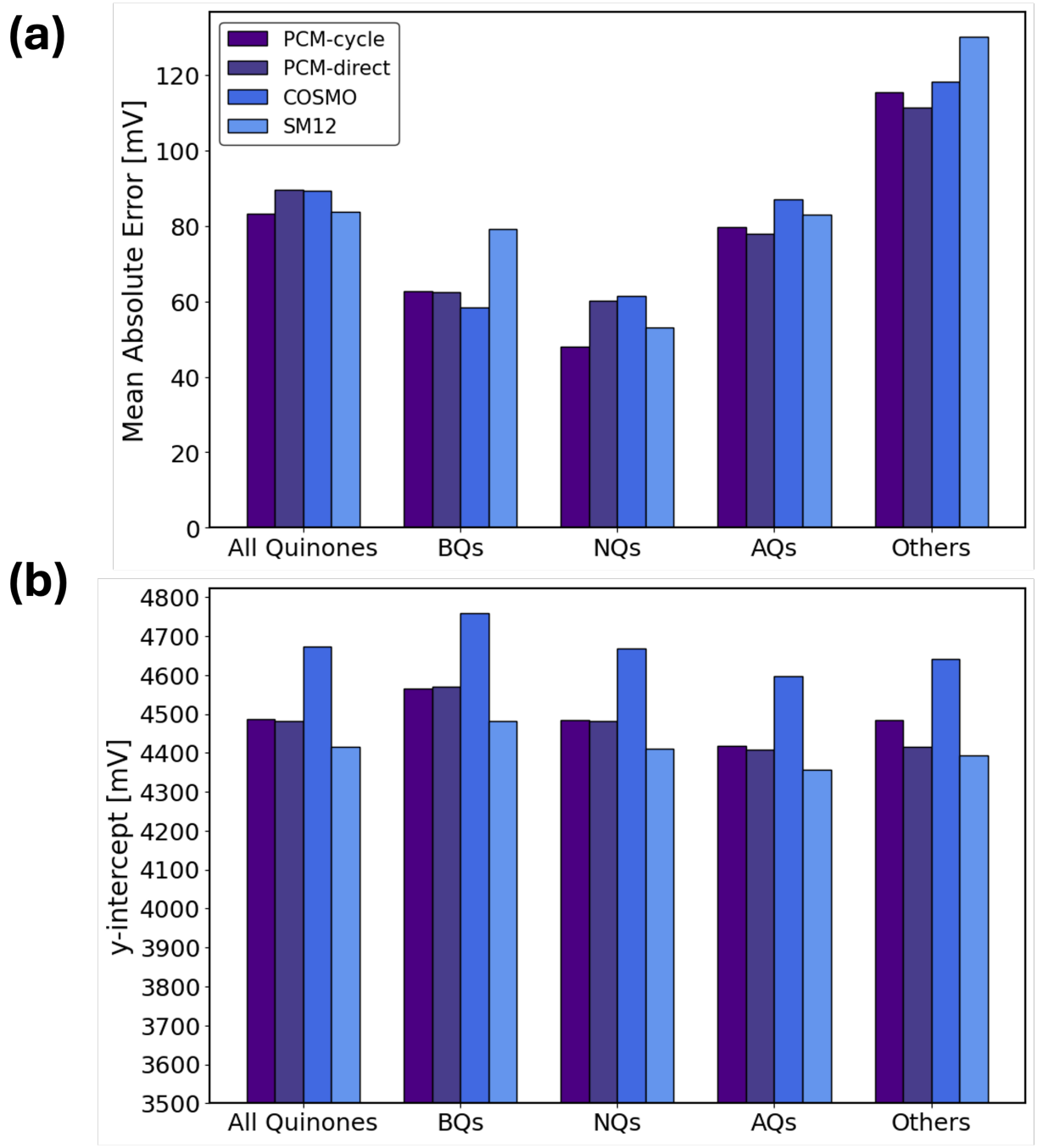

Figure 2: (a) Mean Absolute Errors (MAEs) for the linear regression between computed and experimental $Q/Q^{\bullet-}$ reductions for PCM-cycle, PCM-direct, COSMO, and SM12 considering all quinones or fitting them separately into groups: BQ, NQ, AQ and Others. (b) y-intercepts for the linear regression between computed and experimental $Q/Q^{\bullet-}$ reductions for PCM-cycle, PCM-direct, COSMO, and SM12 considering all quinones or fitting them separately into groups: BQ, NQ, AQ and Others.

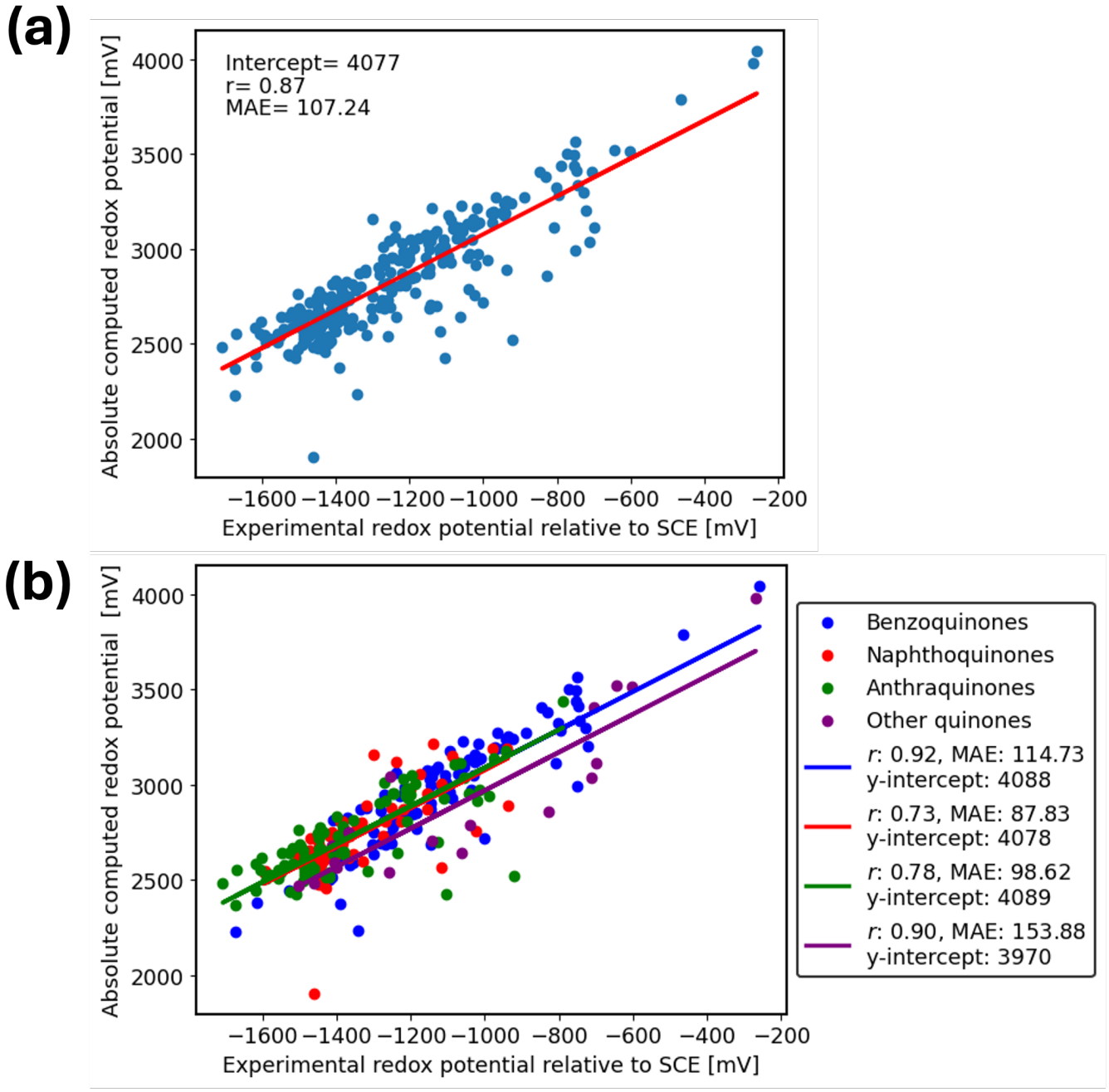

Figure 3: (a) Correlation between $Q^{\bullet-}/Q^{2-}$ experimental reduction potentials relative to SCE and absolute calculated reduction potentials for N = 265 total studied quinone derivatives in DMF using the **PCM-cycle** approach. (b) Correlation between experimental reduction potentials and absolute calculated ones fitted separately for 4 groups: 89 Benzoquinones (blue), 75 Naphthoquinones (red), 83 Anthraquinones (green), and 18 Others (purple). Experimental data were obtained from Prince *et al.*[29]

$Q^{\bullet-}/Q^{2-}$ Reduction Potentials

The correlation between experimental $Q^{\bullet-}/Q^{2-}$ reduction potentials relative to the SCE and the absolute computed reduction potentials is shown in Fig. 3. Compared to the first reduction $Q/Q^{\bullet-}$, there are several notable differences in the quality of the computations for the second reduction potentials $Q^{\bullet-}/Q^{2-}$. First, the $Q^{\bullet-}/Q^{2-}$ linear regression y-intercepts are reduced by almost 400 mV compared to $Q/Q^{\bullet-}$. This is indicative of a large difference in the systematic errors of the two data sets. Second, the Pearson correlation coefficient r is smaller for the $Q^{\bullet-}/Q^{2-}$ data compared to those of $Q/Q^{\bullet-}$. This indicates a larger random error for the second reduction compared to the first reduction. Those random and systematic errors are explored further through the PCM direct and by using other solvation models.

One likely source of random error in the case of second reduction is the lower stability of both species involved in the reduction. $Q^{\bullet-}$ is a radical anion, which is already negatively charged. Further reduction leads to a doubly charged dianion Q^{2-}. Those species do not always remain stable in DMF, as reflected by the fact that reduction potentials could not be measured for all 350 molecules in the Prince *et al.* cyclic voltammetry experiments.[29] When using the thermodynamic cycle, the $Q^{\bullet-}$ and Q^{2-} electronic structures and geometries are optimized in the gas phase where, in the absence of stabilizing interactions of a solvent or counterion, they may be metastable with frontier orbitals embedded in a continuum of other nearby virtual states.[101] This also manifested in SCF convergence issues for the computations, particularly for the di-anions, which had to be resolved using varying SCF convergence algorithms. This led to some clear outliers in the data. One example, molecule 295 (2-hydroxy-3-(10-bromodecyl)-1,4-naphthoquinone), has an absolute error of 711 mV in PCM-cycle compared to the experiment. The source of the error is that the SCF algorithm converged to a wave function where the reducing electron was added to the Br orbital instead of the aromatic quinone ring, resulting in an optimized structure where the bromine group detaches from the rest of the molecule (see Fig. 4).

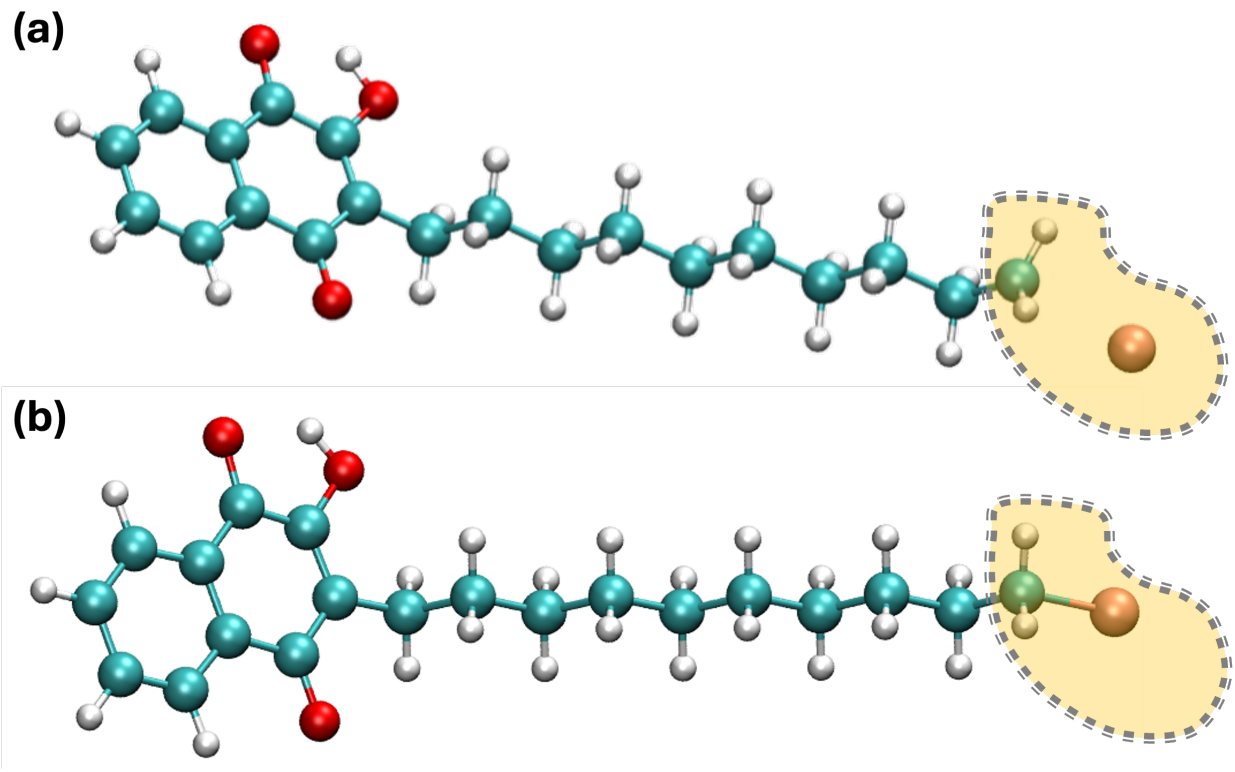

Figure 4: (a) Structure of the 2-hydroxy-3-(10-bromodecyl)-1,4-naphthoquinone di-anion (molecule ID 295) optimized in the gas phase. This structure was used for single-point solvation energy calculations for PCM-cycle, COSMO, and SM12. (b) The same system optimized in the continuum solvent reaction field and used in PCM-direct.

To mitigate errors stemming from SCF convergence in PCM-cycle, we test the PCM-direct approach, where the SCF algorithm and geometry optimizations are carried out in the stabilizing effect of the solvent reaction field instead of the gas phase (see Fig. 5.[102] Overall, this led to improved SCF convergence in most cases, as well as a small improvement in the r value for the overall fit. For some specific molecules, the reduction in error was dramatic. With the PCM-direct approach, the absolute error for molecule 295 is 42 mV, compared to the 711 mV error using PCM-cycle (Fig. 4). This is consistent with studies showing that optimizing molecules directly in solvent usually only has a limited effect unless there are significant structural changes induced by the solvation.[103] Here, the structural changes stem from the difference in the SCF convergence in the gas phase compared to the

PCM.

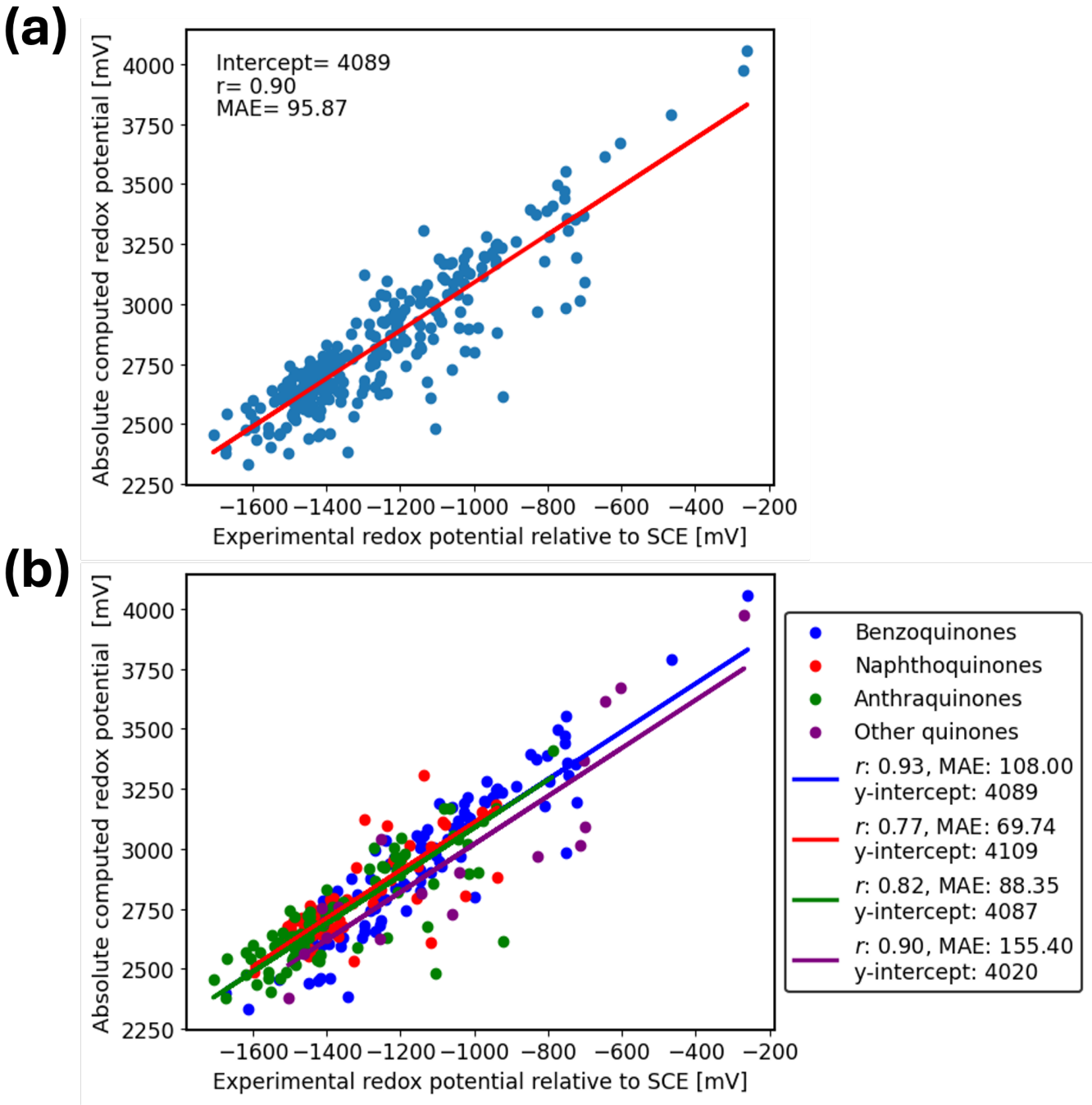

Figure 5: (a) Correlation between $Q^{\bullet-}/Q^{2-}$ experimental reduction potentials relative to SCE and absolute calculated reduction potentials for N = 265 total studied quinone derivatives in DMF using the **PCM-direct** approach. (b) Correlation between experimental reduction potentials and absolute calculated ones fitted separately for 4 groups: 89 Benzoquinones (blue), 75 Naphthoquinones (red), 83 Anthraquinones (green), and 18 Others (purple). Experimental data were obtained from Prince *et al.*[29]

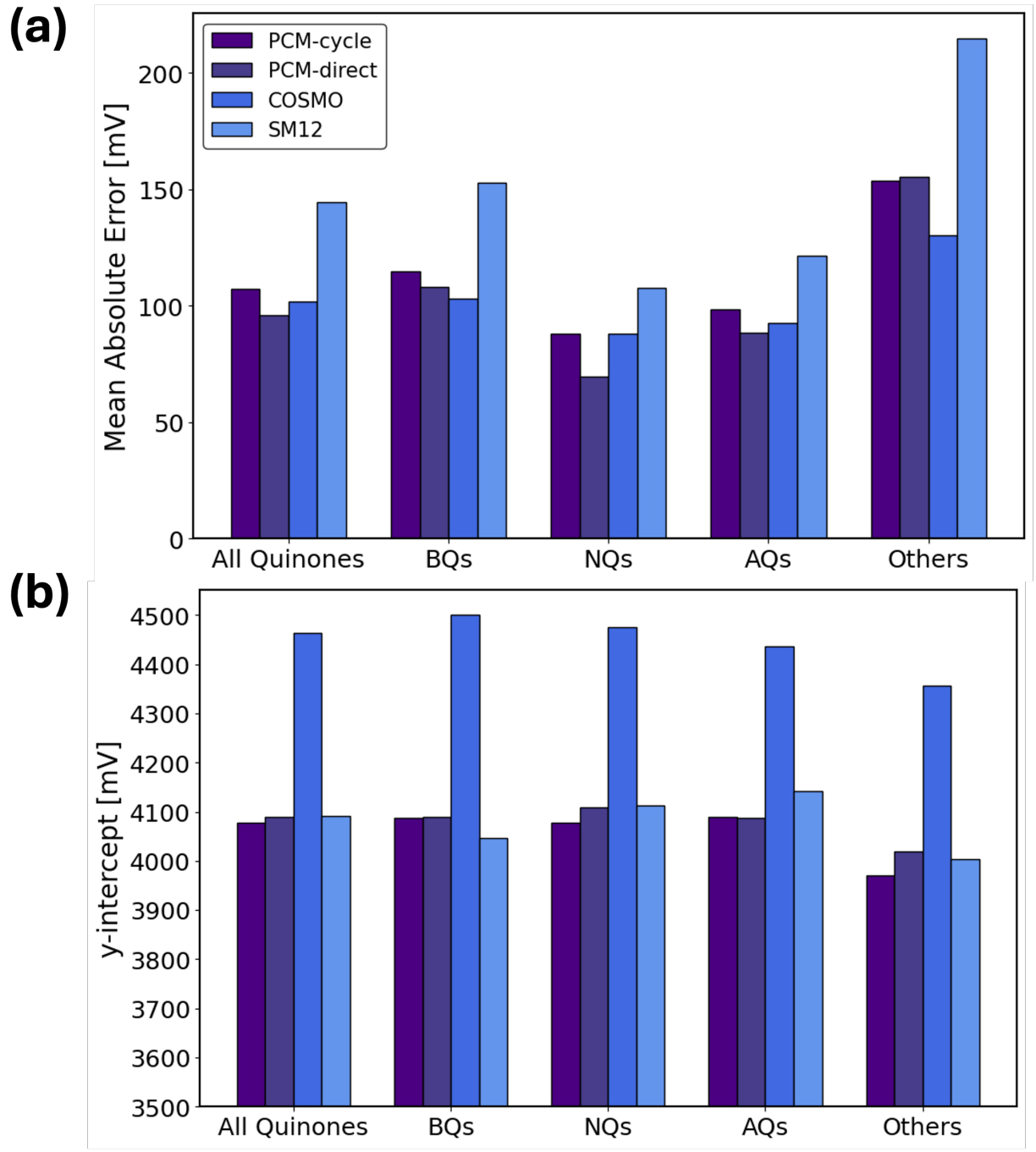

Figure 6: (a) Mean Absolute Error (MAE) for the linear regression between computed and experimental $Q^{\bullet-}/Q^{2-}$ reduction potentials for PCM-cycle, PCM-direct, COSMO, and SM12 considering all quinones or fitting them separately into groups: BQ, NQ, AQ and Others. (b) y-intercept for the linear regression between computed and experimental $Q^{\bullet-}/Q^{2-}$ reduction potentials for PCM-cycle, PCM-direct, COSMO, and SM12 considering all quinones or fitting them separately into groups: BQ, NQ, AQ and Others.

The linear regression for $Q^{\bullet-}/Q^{2-}$ reduction potentials using the PCM-cycle without setting the slope to 1 is shown in SI Fig. S5. The slopes for the individual subgroups decrease in the order BQ > NQ > AQ, exactly as in the case for $Q/Q^{\bullet-}$ (Fig. S1). Again, this error may be due to the unequal distribution of titratable and non-titratable residues across the three subgroups.

In Fig. 6, we summarize the results of the linear regression analyses for PCM-cycle, PCM-direct, COSMO, and SM12 for $Q^{\bullet-}/Q^{2-}$ by comparing their MAEs and y-intercepts. The linear regressions, analogous to Fig. 3, are shown in Figures S6 and S7 in the SI.

Overall MAEs for PCM-direct are smaller than those for PCM-cycle because carrying out the optimization in PCM mitigates issues with SCF convergence affecting several molecules. Here, it would be more appropriate to compare COSMO and SM12 with the PCM-cycle data, since in all cases the same gas phase structures were used. For instance, molecule 295 consistently introduces errors across the three solvation models, causing an error relative to the fit of 943 mV in SM12, 791 mV in COSMO, and 711 mV in PCM. When comparing the three solvent models, COSMO gives slightly lower or comparable MAEs to PCM-cycle. On the other hand, SM12 calculations have a higher MAE across all subgroups. This is likely due to the CM5 charge model which is based on a Hirshfeld population analysis that work well for neutral and cationic species but can be problematic for anions.[104] In several high molecular weight outliers, The CM5 charge model did not even converge and it was necessary to use other charge models. This error was not as pronounced in SM12 for the $Q/Q^{\bullet-}$ reduction, where it performed similarly if not better than other solvation models.

In both the $Q/Q^{\bullet-}$ data (Fig. 2) and the $Q^{\bullet-}/Q^{2-}$ data (Fig. 6), we find that the Other molecules (which includes a few quinones and non-quinones) exhibit the largest MAEs across all solvation models. These "Other" molecules have the smallest sample size (N=33 for $Q/Q^{\bullet-}$ and N=18 for $Q^{\bullet-}/Q^{2-}$) and include several sterically-hindered outliers that increase their MAEs for both redox potentials. Focusing on BQs, NQs, and AQs instead, we find a shift in the error trends when we compare their $Q^{\bullet-}/Q^{2-}$ MAEs to those of $Q/Q^{\bullet-}$. For the second

reduction, $Q^{\bullet-}/Q^{2-}$, BQ exhibits the highest MAE across all solvation models. This is likely because its negative charge (-1 for $Q^{\bullet-}$ and -2 for Q^{2-}) is more concentrated on a smaller ring, posing a challenge to implicit solvation models that perform better when solvating more delocalized charges.[60] In general, multiply-charged anions may cause difficulties for both density functional theory, due to self-interaction errors, as well as to solvent continuum models.[105]

Fig. 6(b) shows the y-intercept values for the different solvation models. PCM-cycle, PCM-direct, and SM12 all give similar y-intercepts. However, COSMO again gives a significantly higher intercept value. While this was also true for the $Q/Q^{\bullet-}$ data (Fig. 2), there the difference between COSMO and PCM-cycle was 187 mV; here, the difference is more pronounced, with COSMO giving a y-intercept that is 387 mV above PCM-cycle.

In all solvation models, the y-intercept calculated for the $Q^{\bullet-}/Q^{2-}$ reduction is smaller than that of $Q/Q^{\bullet-}$. Therefore, systematic errors between $Q/Q^{\bullet-}$ and $Q^{\bullet-}/Q^{2-}$ reductions exist for all solvation models. However, this systematic error appears smallest for COSMO, which gives a $Q^{\bullet-}/Q^{2-}$ y-intercept of 4464 mV compared to a $Q/Q^{\bullet-}$ y-intercept of 4673 mV, a difference of 209 mV. For the other two solvation models, this difference is closer to 400 mV.

Conclusion

This benchmark of 610 reduction potentials from 345 quinones indicates several sources of systematic and random errors. The most prominent systematic error comes from the difference between the first reduction potential ($Q/Q^{\bullet-}$) and the second reduction potential ($Q^{\bullet-}/Q^{2-}$). The latter potentials are lower than the first by around 400 mV with the PCM and SM12 models. COSMO shrinks this difference to around 200 mV, and therefore appears to have a more balanced description of solvation energies of neutral, anionic, and dianionic molecules compared to the other solvation models. Part of this error may also arise from

self-interaction errors in density functional theory, which is larger for molecules with higher negative charge.

In general, MAEs (indicative of random errors) for $Q^{\bullet-}/Q^{2-}$ reduction potentials are also higher than $Q/Q^{\bullet-}$. Within each group, we find a few sources of systematic error. For $Q/Q^{\bullet-}$, ring size introduces an error which may be attributed to lack of size extensivity of electron affinities computed with density functional theory. A second source of error is the nature of the substituents, with non-titratratle substituents giving lower energies on average than titratable ones. Titratable substituents may undergo protonation or deprotonation events that alter the apparent reduction potential experimentally.

In $Q^{\bullet-}/Q^{2-}$, instability of the dianionic species, sometimes manifesting in SCF convergence issues, is another source of random error. This is partly mitigated by carrying out the SCF convergence in the PCM solvation field. Another source of error is associated with solvation of molecules with higher charge concentration, as seen for instance in BQ Q^{2-} species where the -2 charge is localized on a smaller ring.

While this study still indicates the usefulness of DFT calculations in predicting reduction potentials of quinones, there is still work needed to better understand sources of error. The protocol used to run the calculations has been automated and made available on GitHub for further testing of different wave function methods, density functionals, basis sets, and/or solvation models. Other recent benchmark studies have focused on using a more comprehensive benchmark set that includes a wide range of molecules, we emphasize that there is also value in using a large database of similar molecules (here, 345 quinones) measured under similar conditions to better resolve the sources of random and systematic errors.

Acknowledgement

We are grateful to Prof. Gary Hastings for pointing us to the experimental data used in this work. We also thank Jorge Garcia-Alvarez and Prof. Faraj Hasanayn for useful discussions.

This material is based upon work supported as part of the Atomic-C2E project by the U.S. Department of Energy, Office of Science under Award Number DE-SC-0024716. We used Expanse at SDSC through allocation CHE180027 from the Advanced Cyberinfrastructure Coordination Ecosystem: Services and Support (ACCESS) program, which is supported by National Science Foundation grants #2138259, #2138286, #2138307, #2137603, and #2138296. We also acknowledge the use of Advanced Research Computing Technology and Innovation Core (ARCTIC) resources at Georgia State University's Research Solutions made available by the National Science Foundation Major Research Instrumentation (MRI) grant number CNS-1920024.

Supporting Information Available

Linear regression analysis of $Q/Q^{\bullet-}$ and $Q^{\bullet-}/Q^{2-}$ absolute reduction potentials against experimentally determined reduction potentials relative to SCE for the following methods: PCM-cycle (without constraining the slope to 1), PCM-direct, COSMO, and SM12. Table of all molecule structures included in this benchmark and MAEs for $Q/Q^{\bullet-}$ reduction potentials for molecules with different substituent types (PDF).

Other supporting files and scripts are available on GitHub at https://github.com/gozem-gsu/Redox-Potential-Protocol.

References

(1) Sjulstok, E.; Olsen, J. M. H.; Solov'yov, I. A. Quantifying electron transfer reactions in biological systems: what interactions play the major role? *Scientific reports* **2015**, *5*, 18446.

(2) Winget, P.; Cramer, C. J.; Truhlar, D. G. Computation of equilibrium oxidation

and reduction potentials for reversible and dissociative electron-transfer reactions in solution. *Theoretical Chemistry Accounts* **2004**, *112*, 217–227.

(3) Ravelli, D.; Dondi, D.; Fagnoni, M.; Albini, A. Photocatalysis. A multi-faceted concept for green chemistry. *Chemical Society Reviews* **2009**, *38*, 1999–2011.

(4) Schmermund, L.; Jurkas, V.; Ozgen, F. F.; Barone, G. D.; Buchsenschutz, H. C.; Winkler, C. K.; Schmidt, S.; Kourist, R.; Kroutil, W. Photo-biocatalysis: biotransformations in the presence of light. *Acs Catalysis* **2019**, *9*, 4115–4144.

(5) Lee, S. H.; Choi, D. S.; Kuk, S. K.; Park, C. B. Photobiocatalysis: activating redox enzymes by direct or indirect transfer of photoinduced electrons. *Angewandte Chemie International Edition* **2018**, *57*, 7958–7985.

(6) Harrison, W.; Huang, X.; Zhao, H. Photobiocatalysis for abiological transformations. *Accounts of chemical research* **2022**, *55*, 1087–1096.

(7) Meyer, T. J. Redox Pathways: Applications in Catalysis. *Journal of the Electrochemical Society* **1984**, *131*, 221C.

(8) Liu, J.; Lu, L.; Wood, D.; Lin, S. New redox strategies in organic synthesis by means of electrochemistry and photochemistry. *ACS Central Science* **2020**, *6*, 1317–1340.

(9) Koper, M. T. Theory of multiple proton–electron transfer reactions and its implications for electrocatalysis. *Chemical science* **2013**, *4*, 2710–2723.

(10) Zhan, W.; Alvarez, J.; Crooks, R. M. Electrochemical sensing in microfluidic systems using electrogenerated chemiluminescence as a photonic reporter of redox reactions. *Journal of the American Chemical Society* **2002**, *124*, 13265–13270.

(11) Zhou, H.; Xuanyuan, X.; Lv, X.; Wang, J.; Feng, K.; Chen, C.; Ma, J.; Xing, D. Mechanisms of magnetic sensing and regulating extracellular electron transfer of elec-

troactive bacteria under magnetic fields. *Science of The Total Environment* **2023**, *895*, 165104.

(12) Shu, J.; Tang, D. Recent advances in photoelectrochemical sensing: from engineered photoactive materials to sensing devices and detection modes. *Analytical chemistry* **2019**, *92*, 363–377.

(13) Teng, K.-X.; An, Z.-P.; Niu, L.-Y.; Yang, Q.-Z. A Supramolecular Artificial Light-Harvesting System with Excitation Energy and Electron Transfer. *ACS Materials Letters* **2023**, *6*, 290–297.

(14) Jana, B.; Patra, A. Ultrafast Energy Transfer Followed by Electron Transfer in a Polymeric Nanoantenna-Based Light Harvesting System. *The Journal of Physical Chemistry C* **2018**, *122*, 20144–20152.

(15) Weber, A. Z.; Mench, M. M.; Meyers, J. P.; Ross, P. N.; Gostick, J. T.; Liu, Q. Redox flow batteries: a review. *Journal of applied electrochemistry* **2011**, *41*, 1137–1164.

(16) Kwabi, D. G.; Ji, Y.; Aziz, M. J. Electrolyte lifetime in aqueous organic redox flow batteries: a critical review. *Chemical Reviews* **2020**, *120*, 6467–6489.

(17) Marenich, A. V.; Ho, J.; Coote, M. L.; Cramer, C. J.; Truhlar, D. G. Computational electrochemistry: prediction of liquid-phase reduction potentials. *Physical Chemistry Chemical Physics* **2014**, *16*, 15068–15106.

(18) Ikeda, T.; Kano, K. An electrochemical approach to the studies of biological redox reactions and their applications to biosensors, bioreactors, and biofuel cells. *Journal of Bioscience and Bioengineering* **2001**, *92*, 9–18.

(19) Namazian, M.; Coote, M. L. Accurate calculation of absolute one-electron redox potentials of some para-quinone derivatives in acetonitrile. *The Journal of Physical Chemistry A* **2007**, *111*, 7227–7232.

(20) Fu, Y.; Liu, L.; Yu, H.-Z.; Wang, Y.-M.; Guo, Q.-X. Quantum-chemical predictions of absolute standard redox potentials of diverse organic molecules and free radicals in acetonitrile. *Journal of the American Chemical Society* **2005**, *127*, 7227–7234.

(21) Jinich, A.; Sanchez-Lengeling, B.; Ren, H.; Harman, R.; Aspuru-Guzik, A. A mixed quantum chemistry/machine learning approach for the fast and accurate prediction of biochemical redox potentials and its large-scale application to 315 000 redox reactions. *ACS central science* **2019**, *5*, 1199–1210.

(22) Ding, Y.; Li, Y.; Yu, G. Exploring bio-inspired quinone-based organic redox flow batteries: a combined experimental and computational study. *Chem* **2016**, *1*, 790–801.

(23) Ji, X.; Liu, X.; Li, M.; Shao, S.; Chang, J.; Du, J.; Ma, X.; Feng, X.; Zhu, L.; Yu, X.; others Study of the Redox Potentials of Benzoquinone and Its Derivatives by Combining Electrochemistry and Computational Chemistry. *Journal of Chemical Education* **2021**, *98*, 3019–3025.

(24) Huynh, M. T.; Anson, C. W.; Cavell, A. C.; Stahl, S. S.; Hammes-Schiffer, S. Quinone 1 e–and 2 e–/2 H+ reduction potentials: Identification and analysis of deviations from systematic scaling relationships. *Journal of the American Chemical Society* **2016**, *138*, 15903–15910.

(25) Li, Q.; Batchelor-McAuley, C.; Lawrence, N. S.; Hartshorne, R. S.; Compton, R. G. Electrolyte tuning of electrode potentials: the one electron vs. two electron reduction of anthraquinone-2-sulfonate in aqueous media. *Chemical Communications* **2011**, *47*, 11426–11428.

(26) Guin, P. S.; Das, S.; Mandal, P.; others Electrochemical reduction of quinones in different media: a review. *International Journal of Electrochemistry* **2011**, *2011*.

(27) Nohl, H.; Jordan, W.; Youngman, R. J. Quinones in Biology: Functions in electron transfer and oxygen activation. *Advances in Free Radical Biology Medicine* **1986**, *2*, 211–279.

(28) Hastings, G.; Hoshina, S.; Webber, A. N.; Blankenship, R. E. Universality of energy and electron transfer processes in photosystem I. *Biochemistry* **1995**, *34*, 15512–15522.

(29) Prince, R. C.; Dutton, P. L.; Gunner, M. The aprotic electrochemistry of quinones. *Biochimica et Biophysica Acta (BBA) - Bioenergetics* **2022**, *1863*, 148558.

(30) Smith, M. T. Quinones as mutagens, carcinogens, and anticancer agents: introduction and overview. **1985**,

(31) El-Najjar, N.; Gali-Muhtasib, H.; Ketola, R. A.; Vuorela, P.; Urtti, A.; Vuorela, H. The chemical and biological activities of quinones: overview and implications in analytical detection. *Phytochemistry Reviews* **2011**, *10*, 353–370.

(32) Rahman, M. M.; Islam, M. R.; Akash, S.; Shohag, S.; Ahmed, L.; Supti, F. A.; Rauf, A.; Aljohani, A. S.; Al Abdulmonem, W.; Khalil, A. A.; Sharma, R.; Thiruvengadam, M. Naphthoquinones and derivatives as potential anticancer agents: An updated review. *Chemico-Biological Interactions* **2022**, *368*, 110198.

(33) Chien, S.-C.; Wu, Y.-C.; Chen, Z.-W.; Yang, W.-C.; others Naturally occurring anthraquinones: chemistry and therapeutic potential in autoimmune diabetes. *Evidence-Based Complementary and Alternative Medicine* **2015**, *2015*.

(34) ZHOU, P.; Zhao, C.-c.; Li, J.; Zhang, M.; Shi, H.; Wang, L. A review on the role of quinones in cardiovascular disease via inhibiting nlrp3 inflammasome. *Acta Pol. Pharm* **2021**, *78*, 743–748.

(35) Madeo, J.; Zubair, A.; Marianne, F. A review on the role of quinones in renal disorders. *Springerplus* **2013**, *2*, 1–8.

(36) Gerhardt, M. R.; Tong, L.; Gómez-Bombarelli, R.; Chen, Q.; Marshak, M. P.; Galvin, C. J.; Aspuru-Guzik, A.; Gordon, R. G.; Aziz, M. J. Anthraquinone derivatives in aqueous flow batteries. *Advanced energy materials* **2017**, *7*, 1601488.

(37) Jing, Y.; Fell, E. M.; Wu, M.; Jin, S.; Ji, Y.; Pollack, D. A.; Tang, Z.; Ding, D.; Bahari, M.; Goulet, M.-A.; others Anthraquinone flow battery reactants with nonhydrolyzable water-solubilizing chains introduced via a generic cross-coupling method. *ACS Energy Letters* **2021**, *7*, 226–235.

(38) Dulo, B.; Phan, K.; Githaiga, J.; Raes, K.; De Meester, S. Natural quinone dyes: a review on structure, extraction techniques, analysis and application potential. *Waste and Biomass Valorization* **2021**, *12*, 6339–6374.

(39) Kristensen, S. B.; van Mourik, T.; Pedersen, T. B.; Sørensen, J. L.; Muff, J. Simulation of electrochemical properties of naturally occurring quinones. *Scientific reports* **2020**, *10*, 13571.

(40) El-Hag, A.; Al-Jabri, A.; Habbal, O. Antimicrobial properties of Lawsonia inermis (henna): a review. 2007.

(41) Egan, J. M.; Rickenbach, M.; Mooney, K. E.; Palenik, C. S.; Golombeck, R.; Mueller, K. T. Bank Security Dye Packs: Synthesis, Isolation, and Characterization of Chlorinated Products of Bleached 1-(methylamino) anthraquinone. *Journal of forensic sciences* **2006**, *51*, 1276–1283.

(42) Sviatenko, L.; Isayev, O.; Gorb, L.; Hill, F.; Leszczynski, J. Toward robust computational electrochemical predicting the environmental fate of organic pollutants. *Journal of Computational Chemistry* **2011**, *32*, 2195–2203.

(43) Neugebauer, H.; Bohle, F.; Bursch, M.; Hansen, A.; Grimme, S. Benchmark Study of Electrochemical Redox Potentials Calculated with Semiempirical and DFT Methods. *The Journal of Physical Chemistry A* **2020**, *124*, 7166–7176, PMID: 32786975.

(44) Kim, H.; Goodson III, T.; Zimmerman, P. M. Achieving accurate reduction potential predictions for anthraquinones in water and aprotic solvents: Effects of inter-and intramolecular H-bonding and ion pairing. *The Journal of Physical Chemistry C* **2016**, *120*, 22235–22247.

(45) Ghosh, D.; Roy, A.; Seidel, R.; Winter, B.; Bradforth, S.; Krylov, A. I. First-principle protocol for calculating ionization energies and redox potentials of solvated molecules and ions: Theory and application to aqueous phenol and phenolate. *The Journal of Physical Chemistry B* **2012**, *116*, 7269–7280.

(46) Tazhigulov, R. N.; Bravaya, K. B. Free energies of redox half-reactions from first-principles calculations. *The Journal of Physical Chemistry Letters* **2016**, *7*, 2490–2495.

(47) Gordon, M. S.; Freitag, M. A.; Bandyopadhyay, P.; Jensen, J. H.; Kairys, V.; Stevens, W. J. The effective fragment potential method: A QM-based MM approach to modeling environmental effects in chemistry. *The Journal of Physical Chemistry A* **2001**, *105*, 293–307.

(48) Hruska, E.; Gale, A.; Liu, F. Bridging the experiment-calculation divide: Machine learning corrections to redox potential calculations in implicit and explicit solvent models. *Journal of Chemical Theory and Computation* **2022**, *18*, 1096–1108.

(49) Marenich, A. V.; Olson, R. M.; Kelly, C. P.; Cramer, C. J.; Truhlar, D. G. Self-consistent reaction field model for aqueous and nonaqueous solutions based on accurate polarized partial charges. *Journal of Chemical Theory and Computation* **2007**, *3*, 2011–2033.

(50) Becke, A. D. Density-functional exchange-energy approximation with correct asymptotic behavior. *Physical review A* **1988**, *38*, 3098.

(51) Lee, C.; Yang, W.; Parr, R. G. Development of the Colle-Salvetti correlation-energy formula into a functional of the electron density. *Physical review B* **1988**, *37*, 785.

(52) Hehre, W. J.; Ditchfield, R.; Pople, J. A. Self—consistent molecular orbital methods. XII. Further extensions of Gaussian—type basis sets for use in molecular orbital studies of organic molecules. *The Journal of Chemical Physics* **1972**, *56*, 2257–2261.

(53) Kitheka, M. M.; Redington, M.; Zhang, J.; Yao, Y.; Goyal, P. Benchmarks of the density functional tight-binding method for redox, protonation and electronic properties of quinones. *Physical Chemistry Chemical Physics* **2022**, *24*, 6742–6756.

(54) Frontana, C.; Vázquez-Mayagoitia, Á.; Garza, J.; Vargas, R.; González, I. Substituent effect on a family of quinones in aprotic solvents: an experimental and theoretical approach. *The Journal of Physical Chemistry A* **2006**, *110*, 9411–9419.

(55) Weigend, F.; Ahlrichs, R. Balanced basis sets of split valence, triple zeta valence and quadruple zeta valence quality for H to Rn: Design and assessment of accuracy. *Phys. Chem. Chem. Phys.* **2005**, *7*, 3297–3305.

(56) Barone, V.; Cossi, M.; Tomasi, J. A new definition of cavities for the computation of solvation free energies by the polarizable continuum model. *The Journal of chemical physics* **1997**, *107*, 3210–3221.

(57) Cossi, M.; Barone, V.; Cammi, R.; Tomasi, J. Ab initio study of solvated molecules: a new implementation of the polarizable continuum model. *Chemical Physics Letters* **1996**, *255*, 327–335.

(58) Tomasi, J.; Mennucci, B.; Cammi, R. Quantum mechanical continuum solvation models. *Chemical reviews* **2005**, *105*, 2999–3094.

(59) Klamt, A.; Schüürmann, G. COSMO: a new approach to dielectric screening in solvents with explicit expressions for the screening energy and its gradient. *Journal of the Chemical Society, Perkin Transactions 2* **1993**, 799–805.

(60) Cramer, C. J.; Truhlar, D. G. A universal approach to solvation modeling. *Accounts of chemical research* **2008**, *41*, 760–768.

(61) Marenich, A. V.; Cramer, C. J.; Truhlar, D. G. Generalized Born Solvation Model SM12. *Journal of Chemical Theory and Computation* **2013**, *9*, 609–620, PMID: 26589059.

(62) Ho, J.; Coote, M. L.; Cramer, C. J.; Truhlar, D. G. 6 Theoretical Calculation of Reduction Potentials. **2015**,

(63) Frisch, M. J. et al. Gaussian˜16 Revision C.01. 2016; Gaussian Inc. Wallingford CT.

(64) Epifanovsky, E. et al. Software for the frontiers of quantum chemistry: An overview of developments in the Q-Chem 5 package. *The Journal of Chemical Physics* **2021**, *155*, 084801.

(65) Marenich, A. V.; Jerome, S. V.; Cramer, C. J.; Truhlar, D. G. Charge Model 5: An Extension of Hirshfeld Population Analysis for the Accurate Description of Molecular Interactions in Gaseous and Condensed Phases. *Journal of Chemical Theory and Computation* **2012**, *8*, 527–541, PMID: 26596602.

(66) Winget, P.; Dolney, D. M.; Giesen, D. J.; Cramer, C. J.; Truhlar, D. G. Minnesota solvent descriptor database. *Minneapolis, MN: Department of Chemistry and Supercomputer Institute* **1999**,

(67) Bacskay, G. B. A quadratically convergent Hartree—Fock (QC-SCF) method. Application to closed shell systems. *Chemical Physics* **1981**, *61*, 385–404.

(68) Singh, U. C.; Kollman, P. A. A combined ab initio quantum mechanical and molecular mechanical method for carrying out simulations on complex molecular systems: Applications to the CH3Cl + Cl exchange reaction and gas phase protonation of polyethers. *Journal of Computational Chemistry* **1986**, *7*, 718–730.

(69) Besler, B. H.; Merz Jr., K. M.; Kollman, P. A. Atomic charges derived from semiempirical methods. *Journal of Computational Chemistry* **1990**, *11*, 431–439.

(70) Breneman, C. M.; Wiberg, K. B. Determining atom-centered monopoles from molecular electrostatic potentials. The need for high sampling density in formamide conformational analysis. *Journal of Computational Chemistry* **1990**, *11*, 361–373.

(71) Kelly, C. P.; Cramer, C. J.; Truhlar, D. G. Aqueous Solvation Free Energies of Ions and IonWater Clusters Based on an Accurate Value for the Absolute Aqueous Solvation Free Energy of the Proton. *The Journal of Physical Chemistry B* **2006**, *110*, 16066–16081, PMID: 16898764.

(72) Konezny, S. J.; Doherty, M. D.; Luca, O. R.; Crabtree, R. H.; Soloveichik, G. L.; Batista, V. S. Reduction of systematic uncertainty in DFT redox potentials of transition-metal complexes. *The Journal of Physical Chemistry C* **2012**, *116*, 6349–6356.

(73) Truhlar, D. G.; Cramer, C. J.; Lewis, A.; Bumpus, J. A. Molecular modeling of environmentally important processes: Reduction potentials. *Journal of Chemical Education* **2004**, *81*, 596.

(74) Isse, A. A.; Gennaro, A. Absolute potential of the standard hydrogen electrode and the problem of interconversion of potentials in different solvents. *The Journal of Physical Chemistry B* **2010**, *114*, 7894–7899.

(75) Trasatti, S. The "absolute" electrode potential—The end of the story. *Electrochimica Acta* **1990**, *35*, 269–271.

(76) Jinnouchi, R.; Anderson, A. B. Aqueous and surface redox potentials from self-consistently determined Gibbs energies. *The Journal of Physical Chemistry C* **2008**, *112*, 8747–8750.

(77) Inzelt, G.; Lewenstam, A.; Scholz, F. *Handbook of reference electrodes*; Springer, 2013; Vol. 541.

(78) Tripkovic, V.; Björketun, M. E.; Skúlason, E.; Rossmeisl, J. Standard hydrogen electrode and potential of zero charge in density functional calculations. *Physical Review B* **2011**, *84*, 115452.

(79) Tomanik, L.; Rulisek, L.; Slavicek, P. Redox Potentials with COSMO-RS: Systematic Benchmarking with Different Databases. *Journal of Chemical Theory and Computation* **2023**, *19*, 1014–1022.

(80) Busch, M.; Ahlberg, E.; Laasonen, K. From absolute potentials to a generalized computational standard hydrogen electrode for aqueous and non-aqueous solvents. *Physical Chemistry Chemical Physics* **2021**, *23*, 11727–11737.

(81) The absolute electrode potential: an explanatory note (Recommendations 1986). *Journal of Electroanalytical Chemistry and Interfacial Electrochemistry* **1986**, *209*, 417–428.

(82) Kelly, C. P.; Cramer, C. J.; Truhlar, D. G. Single-Ion Solvation Free Energies and the Normal Hydrogen Electrode Potential in Methanol, Acetonitrile, and Dimethyl Sulfoxide. *The Journal of Physical Chemistry B* **2007**, *111*, 408–422, PMID: 17214493.

(83) Matsui, T.; Kitagawa, Y.; Okumura, M.; Shigeta, Y. Accurate standard hydrogen electrode potential and applications to the redox potentials of vitamin C and NAD/NADH. *The Journal of Physical Chemistry A* **2015**, *119*, 369–376.

(84) Donald, W. A.; Leib, R. D.; Demireva, M.; O'Brien, J. T.; Prell, J. S.; Williams, E. R. Directly Relating Reduction Energies of Gaseous Eu (H2O) n 3+, n= 55- 140, to Aqueous Solution: The Absolute SHE Potential and Real Proton Solvation Energy. *Journal of the American Chemical Society* **2009**, *131*, 13328–13337.

(85) Donald, W. A.; Leib, R. D.; O'Brien, J. T.; Bush, M. F.; Williams, E. R. Absolute standard hydrogen electrode potential measured by reduction of aqueous nanodrops in the gas phase. *Journal of the American Chemical Society* **2008**, *130*, 3371–3381.

(86) Donald, W. A.; Demireva, M.; Leib, R. D.; Aiken, M. J.; Williams, E. R. Electron hydration and ion- electron pairs in water clusters containing trivalent metal ions. *Journal of the American Chemical Society* **2010**, *132*, 4633–4640.

(87) Matsui, T.; Kitagawa, Y.; Okumura, M.; Shigeta, Y.; Sakaki, S. Consistent scheme for computing standard hydrogen electrode and redox potentials. *Journal of Computational Chemistry* **2013**, *34*, 21–26.

(88) Gritzner, G.; Kuta, J. Recommendations on reporting electrode potentials in non-aqueous solvents (Recommendations 1983). *Pure and Applied Chemistry* **1984**, *56*, 461–466.

(89) Baik, M.-H.; Friesner, R. A. Computing redox potentials in solution: Density functional theory as a tool for rational design of redox agents. *The Journal of Physical Chemistry A* **2002**, *106*, 7407–7412.

(90) Diggle, J.; Parker, A. Liquid junction potentials in electrochemical cells involving a dissimilar solvent junction. *Australian Journal of Chemistry* **1974**, *27*, 1617–1621.

(91) Makoś, M. Z.; Gurunathan, P. K.; Raugei, S.; Kowalski, K.; Glezakou, V.-A.; Rousseau, R. Modeling Absolute Redox Potentials of Ferrocene in the Condensed Phase. *The Journal of Physical Chemistry Letters* **2022**, *13*, 10005–10010, PMID: 36264148.

(92) Namazian, M.; Lin, C. Y.; Coote, M. L. Benchmark calculations of absolute reduction potential of ferricinium/ferrocene couple in nonaqueous solutions. *Journal of chemical theory and computation* **2010**, *6*, 2721–2725.

(93) Nørskov, J. K.; Rossmeisl, J.; Logadottir, A.; Lindqvist, L.; Kitchin, J. R.; Bligaard, T.; Jonsson, H. Origin of the overpotential for oxygen reduction at a fuel-cell cathode. *The Journal of Physical Chemistry B* **2004**, *108*, 17886–17892.

(94) Cheng, J.; Liu, X.; VandeVondele, J.; Sulpizi, M.; Sprik, M. Redox potentials and acidity constants from density functional theory based molecular dynamics. *Accounts of Chemical Research* **2014**, *47*, 3522–3529.

(95) Speelman, A. L.; Gillmore, J. G. Efficient computational methods for accurately predicting reduction potentials of organic molecules. *The Journal of Physical Chemistry A* **2008**, *112*, 5684–5690.

(96) RDKit: Open-source cheminformatics software. `https://www.rdkit.org/`, Accessed: March 21st, 2024.

(97) Pedregosa, F. et al. Scikit-learn: Machine Learning in Python. *Journal of Machine Learning Research* **2011**, *12*, 2825–2830.

(98) Bard, A. J.; Faulkner, L. R.; White, H. S. *Electrochemical methods: fundamentals and applications*; John Wiley & Sons, 2022.

(99) Whittleton, S. R.; Sosa Vazquez, X. A.; Isborn, C. M.; Johnson, E. R. Density-functional errors in ionization potential with increasing system size. *The Journal of Chemical Physics* **2015**, *142*, 184106.

(100) Hui, Y.; Chng, E. L. K.; Chng, C. Y. L.; Poh, H. L.; Webster, R. D. Hydrogen-Bonding Interactions between Water and the One- and Two-Electron-Reduced Forms of Vitamin K1: Applying Quinone Electrochemistry To Determine the Moisture Content of Non-Aqueous Solvents. *Journal of the American Chemical Society* **2009**, *131*, 1523–1534, PMID: 19132833.

(101) Zhao, H.; Zhou, J.; Jena, P. Stability of B12 (CN) 122-: implications for lithium and magnesium ion batteries. *Angewandte Chemie* **2016**, *128*, 3768–3772.

(102) Ren, F.; Liu, F. Impacts of polarizable continuum models on the SCF convergence and DFT delocalization error of large molecules. *The Journal of Chemical Physics* **2022**, *157*.

(103) Ho, J.; Ertem, M. Z. Calculating free energy changes in continuum solvation models. *The Journal of Physical Chemistry B* **2016**, *120*, 1319–1329.

(104) Peeples, C. A.; Schreckenbach, G. Implementation of the SM12 Solvation Model into ADF and Comparison with COSMO. *Journal of Chemical Theory and Computation* **2016**, *12*, 4033–4041, PMID: 27322858.

(105) Falbo, E.; Penfold, T. J. Redox Potentials of Polyoxometalates from an Implicit Solvent Model and QM/MM Molecular Dynamics. *The Journal of Physical Chemistry C* **2020**, *124*, 15045–15056.